ACS OMEGA

Open Access

http://pubs.acs.org/journal/acsodf

Article

Selective Labeling of Small Microplastics with SERS-Tags Based on Gold Nanostars: Method Optimization Using Polystyrene Beads and Application in Environmental Samples

Anna Mercedi, Giulia Gentili, Valentina Poli, Carolin Philipp, Beatrice Rosso, Maria Cristina Lavagnolo, Ingeborg Hallanger, Fabiana Corami, Moreno Meneghetti, and Lucio Litti*

Cite This: *ACS Omega* 2024, 9, 40821−40831

Read Online

ACCESS | Metrics & More | Article Recommendations | Supporting Information

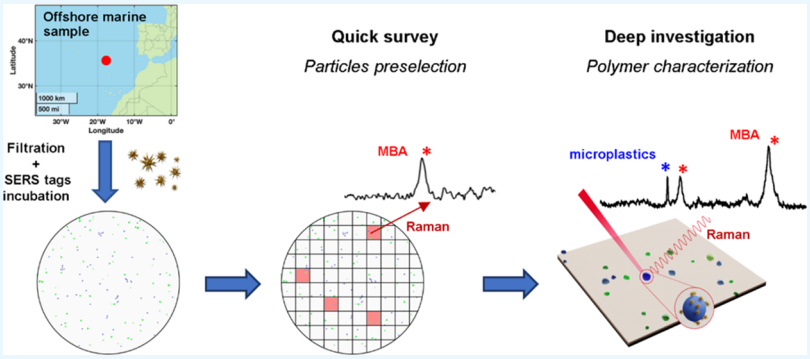

ABSTRACT: Microplastics pollution is being unanimously recognized as a global concern in all environments. Routine analysis protocols foresee that samples, which are supposed to contain up to hundreds of microplastics, are eventually collected on nanoporous filters and inspected by microspectroscopy techniques like micro-FTIR or micro-Raman. All particles, whether made of plastic or not, must be inspected one by one to detect and count microplastics. This makes it extremely time-consuming, especially when Raman is adopted, and indeed mandatory for the small microplastic fraction. Inspired by the principles of cell labeling, the present study represents the first report in which gold nanostars (AuNS) are functionalized to act as SERS-tags and used to selectively couple to microplastics. The intrinsic bright signals provided by the SERS-tags are used to run a quick scan over a wide filter area with roughly 2 orders of magnitude shorter analysis time in respect of state of the art in micro- and nanoplastics detection by μ-Raman. The applicability of the present protocol has been validated at the proof-of-concept level on both fabricated and real offshore marine samples. It is indeed worth mentioning that a SERS-based approach is herein successfully applied on filters and protocols routinely adopted in environmental microplastics monitoring, paving the way for future implementations and applications.

1. INTRODUCTION

As a result of increased plastic manufacturing and anthropogenic activities, plastic waste has become a widespread and growing concern worldwide.[1] Exposure to ultraviolet (UV) radiation, elevated temperatures, mechanical forces (wind or waves), and atmospheric oxygen can cause the plastic to degrade and fragment to smaller dimension particles, called microplastics.[2−4] While "small microplastics are usually intended below 10 μm, the World Health Organization defines nanoplastics as particles of dimensions between 1 nm and 1 μm.[5] They have gained scientific and public attention due to their accumulation and effects on the environment,[6−9] as well as on human health.[9,10] The ubiquitous nature of these particles has been ascertained since they can be found in almost every environmental compartment,[11−16] in animals,[17−22] food,[23] and human bodies.[24,25] Therefore, the extensive effort devoted to the development of reliable tools and protocols for the filtering, identification, and quantification of micro- and nanoplastics is not surprising. Vibrational spectroscopy, *i.e.* Fourier transform infrared spectroscopy (FT-IR) and Raman spectroscopy, is often employed for the identification of microplastics because of multiple advantages, including nondestructiveness, nonintrusiveness, minimal requirement of sample amount, and potentials for high-throughput screening.[2,26] Additionally, these techniques can be coupled with optical microscopy, allowing both spectroscopical and morphological particles characterization.[27]

Received: June 18, 2024
Revised: August 29, 2024
Accepted: September 2, 2024
Published: September 18, 2024

Raman spectroscopy can achieve higher spatial resolution than FT-IR (down to 0.5−1 μm),[26,28] thanks to the shorter wavelengths employed, and can work in the presence of water.[29] There are, however, some strong limitations with the use of Raman spectroscopy, the most important being interference with fluorescence and long measurement times.[27,29] These long times are intrinsic to the technique but are also due to the fact that the sample contains a huge number of particles, where only a small percentage are actually microplastics.[27] Moreover, the smallest fraction of microplastics and nanoplastics are not easily recognizable by visual inspection and Raman imaging unless more complex and advanced techniques are employed, such as stimulated Raman spectroscopy which, in a recent study, allowed us to detect and identify nanoplastics in bottled water.[30] A common approach for Raman analysis of microplastics is to acquire spectra over an entire area, without a preselection step to determine the location of microparticles.[31,32] This approach is tremendously time-consuming and intrinsically inefficient. To make the analysis more suitable for routine practice, a proper method is needed to preselect the microplastics and nanoplastics, as it was already implemented for μFTIR for microplastics larger than 10 μm.[33] Some approaches that can be used are visual sorting or staining with lipophilic fluorescent dyes, such as Nile Red.[34,35] Visual sorting (manual and software-assisted) is useful to identify larger microplastics (>10−20 μm), but is not as efficient with smaller particles.[36] The same applies to Nile Red staining, which may indeed be detrimental to subsequent Raman analysis due to its fluorescence.[34] Surface enhanced Raman scattering (SERS) is a technique that takes advantage of the huge local field amplification provided by localized surface plasmon resonances supported on metallic nanostructures, such as gold or silver,[37] causing a great enhancement of the Raman signals of molecules located on the metal nanostructures. Due to the bright and fingerprint signals provided by SERS, it has recently been successfully applied in quantitative sensor technology,[38] as well as in cell labeling and counting.[39] The application of SERS techniques for the analysis of microplastics is currently mostly limited to the use of plasmonic surfaces,[40−42] or particles,[43,44] to enhance the Raman signals of selected microplastics,[45,46] whereas, to the best of our knowledge, not any application of SERS as a preselection tool is reported. SERS can facilitate the recognition of smaller microplastics and nanoplastics by enhancing their Raman signals but does not solve the issues related to the preselection of the particles, and the untargeted SERS amplification may result in enhancing the signals of other interferences present in the sample as well. Lastly, SERS techniques for microplastics all require special sample pretreatments of substrates and cannot be directly implemented to preexisting sample preparation techniques or substrate like alumina filters. The hypothesis underlying this study is the implementation of an effective methodology, based on SERS, to overpass the long analysis time needed for micro-Raman inspection of microplastics collected on porous filters.

Herein, the use of plasmonic SERS labels to tag micro- and nanoplastics has been presented for the first time. Despite the direct polymers Raman signal amplification,[47] and the microplastics labeling, are essentially evolution of the same purpose (i.e., microplastic detection), they should not really be defined as the same concept, nor they need the same requisites for been successfully applied. These SERS-tags are made of gold nanostars (AuNS) functionalized with p-mercaptobenzoic acid (MBA), to provide clear and sharp SERS fingerprint and tunable hydrophobicity.[48] AuNS-MBA SERS-tags have strong SERS signals that can be easily recognized during a quick survey at low magnification. The same does not interfere with the Raman spectra of the polymers, which are still clearly recognizable. It is herein demonstrated that a strong selective interaction of AuNS-MBA with polystyrene (PS), low-density polyethylene (LDPE), poly(ethylene terephthalate) (PET), poly(tetrafluoroethylene) (PTFE), polyamide-6 (PA6), and polyamide-12 (PA12) beads, as representative microplastics, can be exploited because of the tunable hydrophobicity of MBA. Silica represents one of the most abundant components of sandy sediments, as well as one of the most common interferences in microplastic analysis by visual inspection.[49] SiO_2 particles of the same dimension are used in preliminary studies as representative of a background derived from nonplastic particles. The performance of this labeling approach has been optimized with fabricated samples containing 800 nm PS beads, as well as on untreated offshore, ocean surface water as an example of practical application. The microplastics were labeled with SERS-tags and filtered on alumina filters, widely adopted in microplastics monitoring campaigns.[50,51] It would be of strategic importance that a new method can integrate well with the most used practices and materials. Due to their selective interactions and the rapid survey allowed by the SERS-tags, small-sized microplastics were located and identified in real environmental samples. Overall, this methodology allows the measurement time to be drastically reduced, especially with small microplastics detected with μ-Raman, which are not efficiently recognized by visual inspection.

2. MATERIALS AND METHODS

2.1. Synthesis of Gold Nanostars. The synthesis of AuNS followed a surfactant-free seed growth method assisted by silver ions.[52−54] 10 mL of pure water, 50 μL of 50 mM $HAuCl_4$ (Sigma-Aldrich), and 10 μL of 1 M HCl (Sigma-Aldrich) were added to a glass vial. 100 μL of gold nanoparticles (AuNP, [Au] = 1.5 mM), 50 μL of 10 mM $AgNO_3$ (Sigma-Aldrich), and 25 μL of 100 mM ascorbic acid (Sigma-Aldrich) were then rapidly added under vigorous stirring. After 1 min, 50 μL of 1 mM para-mercaptobenzoic acid (Sigma-Aldrich) was added to the solution, which was then stirred for another 2 h. The particles were purified by 2-step centrifugation at 1500 RCF for 5 min and redispersed in 5 mL of ultrapure water, obtaining the solution that has been used for the labeling. The nanostars were then characterized by UV−vis−NIR spectroscopy (Agilent Cary 5000) and TEM (FEI Tecnai G2 12 operating at 100 kV), Figure S1. The concentration of nanostars was determined by the UV−vis spectrum of the seeds, with the help of a previously published procedure. Since the spherical nanoparticles act as seed for the growth of the nanostars, the number of nanoparticles added as seed for the reaction can be assumed to be equal to the number of nanostars at the end of the synthesis (Figure S2).[37] Matlab (MathWorks, Inc.), version R2022b, was used for data manipulation and figures preparation.

2.2. Synthesis of Silica Microparticles. Silica microparticles were synthesized via the Stöber method.[55] 5 mL of ethanol, 450 μL of NH_4OH, and 70 μL of stilled water were mixed into a glass vial. The vial was transferred to a 42 °C sonicator bath, and then 1.015 mL of TEOS (tetraethyl orthosilicate, Sigma-Aldrich) was added. The reaction mixture was left under sonication for 2 h, then quenched with 2 mL of

https://doi.org/10.1021/acsomega.4c05693
ACS Omega 2024, 9, 40821−40831

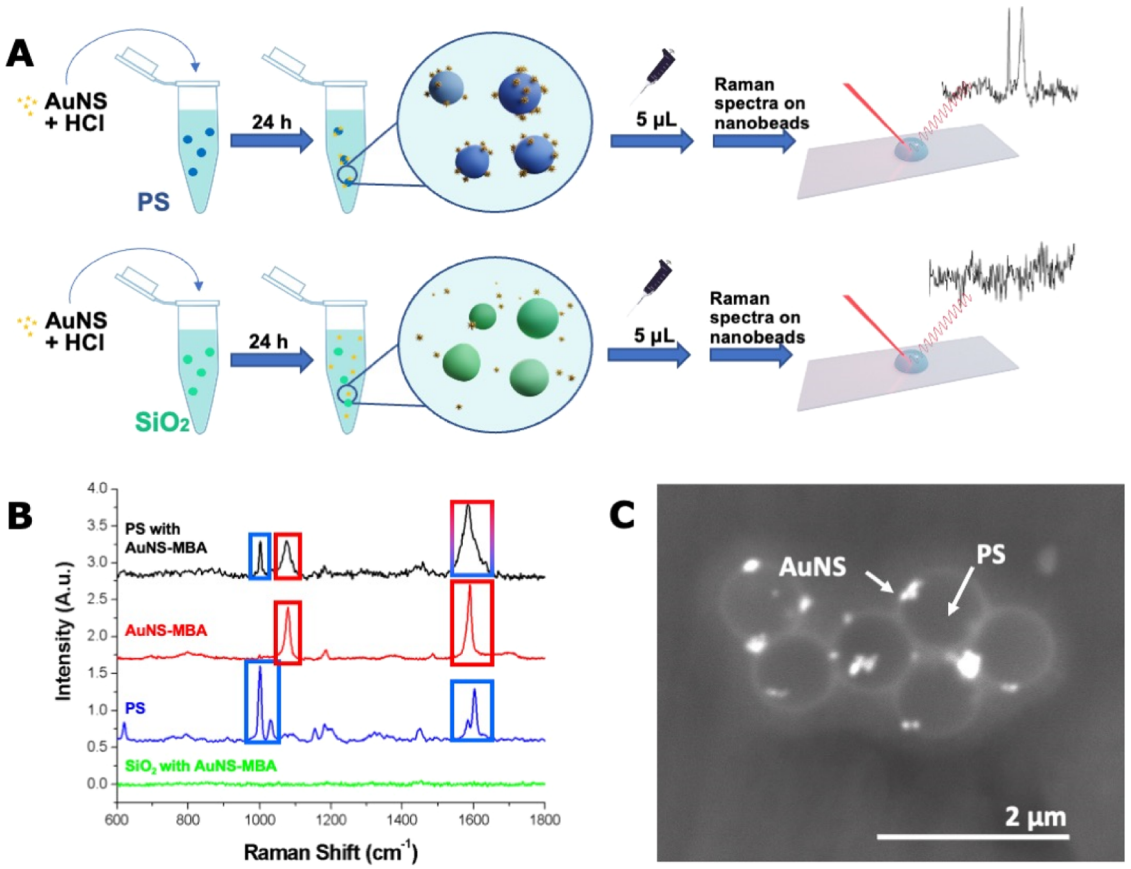

Figure 1. (A) Schematic representation of the method for incubation of AuNS-MBA with PS and SiO_2 nanobeads, and related inspection by μ-Raman; (B) PS, AuNS-MBA, and PS and SiO_2 incubated with AuNS-MBA normalized spectra (SiO_2 beads are recorded on Al foil to avoid interferences by the glass slide); (C) SEM (backscattered electrons) image of AuNS-MBA on the surface of PS spheres.

Milli-Q water. The particles were purified by two-step centrifugation at 17 500 RCF for 3 min and redispersed in Milli-Q water. The mixture was then subjected to another centrifugation step at 500 RCF for 3 min, and the particles were recovered from the supernatant. Particle size was determined by SEM (scanning electron microscope, JSM Jeol 6490, Figure S3).

2.3. Estimation of Particle Concentration. A solution of polystyrene (PS) nanoplastics (800 nm, Figure S3) was prepared by diluting a concentrated suspension (10 wt %, Sigma-Aldrich). The concentration of these solutions (silica and polystyrene) was then determined by manual counting of the particles dropped on a glass surface (refer to the dedicated section in the Supporting Information for details).

2.4. Sample Preparation and SERS Detection on Glass Slide. 30 μL of each particle (polystyrene and silica) solution at 0.12 pM (Table S2) was mixed with 1.5 μL of HCl 0.1 M (to reach a final pH of about 5−6) and with different amounts of AuNS-MBA solution (0, 2, 5, 10, 15, 25, 50 μL), corresponding to a ratio between the number of gold nanostars and the number of PS or SiO_2 particles of 0, 0.93, 2.31, 4.63, 6.94, 11.57, and 23.14. Milli-Q water was added to reach a final volume of 0.3 mL, and the mixtures were vortexed for about 24 h. Finally, 5 μL of each solution was dropped onto a glass surface (Figure 1A), previously cleaned with piranha solution (H_2O_2/H_2SO_4 1:3). The samples were analyzed using a Renishaw InVia μ-Raman microscope. For each drop, about 100−200 particles were identified with a 100x objective (Leica Fluotar, NA = 0.9) and a spectrum was acquired on each particle (wavelength 633 nm, 0.1 mW laser power, 3 s acquisition). Renishaw WiRe 4.4 software was used for the removal of the baseline, and then the spectra were analyzed using Matlab 2019b routines. For each spectrum, the intensity at the characteristic peaks of PS and MBA (1003 and 1078 cm^{-1}, respectively) and Pearson correlations with the respective reference spectra were considered. The samples with the highest ratio of AuNS-MBA over PS or SiO_2 nanobeads were also investigated by μ-Raman imaging: spectra were acquired on two areas of about 100 × 150 μm^2, on a grid of 1 μm edge, with a laser wavelength of 633 nm, 100× (Leica Fluotar NA = 0.9) objective. Baseline removal was done with WiRe 4.4, and then the μ-Raman map was elaborated with Matlab 2019b, based on the intensity at 1078 cm^{-1} (MBA). All experiments were run at ambient temperature. Matlab (MathWorks, Inc.), version R2022b, was used for data manipulation and figures preparation.

2.5. Sample Preparation and SERS Detection on Alumina Filter. A mixture of PS and SiO_2 particles was prepared by mixing silica and PS solution at a 1:1 ratio and 30 μL total volume. Then, 10 μL of AuNS-MBA solution, 1.5 μL of HCl 0.1 M, and 260 μL of Milli-Q water were added. The mixture was vortexed for 24 h. 20 μL was finally filtered on an aluminum oxide filter (0.2 μm, 47 mm diameter, ANODISC Anopore Inorganic Membrane, Whatman, Merck Darmstadt Germany). The first quick μ-Raman imaging scan (hereafter referred to as quick map) was done by using a 10x (N.A. 0.25) objective and 785 nm excitation wavelength on an area of 200 × 200 μm^2 with a step size of 10 μm. Each spectrum was

https://doi.org/10.1021/acsomega.4c05693
ACS Omega 2024, 9, 40821−40831

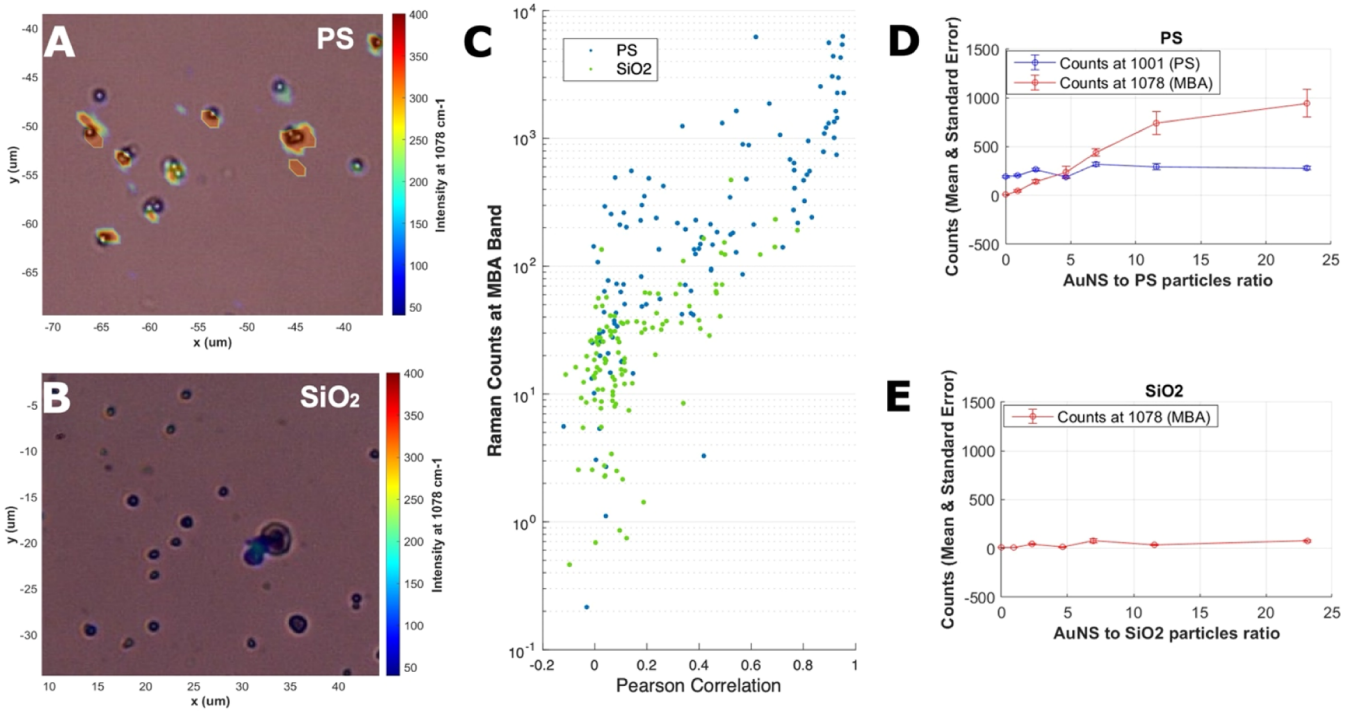

Figure 2. Magnified insets from the μ-Raman imaging of the PS (A) or SiO_2 (B) nanobeads incubated with AuNS-MBA (Figure S6). The false-colored maps are representative of the intensities of the MBA SERS peak at 1078 cm^{-1}. (C) Comparison of MBA signals obtained on PS and SiO_2 particles. The scatter plot represents the Pearson correlation with MBA's reference spectrum over the SERS intensity at 1078 cm^{-1} (MBA's characteristic peak). The number of AuNS-MBA over PS, or SiO_2, nanobeads was set as 12:1. Mean values of the intensity at PS (1003 cm^{-1}) and MBA (1078 cm^{-1}) characteristic peaks measured on polystyrene (D) and mean value of the intensity at 1078 cm^{-1} on silica (E) for different AuNS-MBA to nanobeads ratio. The error bars represent the standard error of the mean.

acquired for 10 s at 3 mW laser power. Baseline correction and cosmic ray removal were done with WiRe 4.4 software, and the results were then elaborated using Matlab R2019b, based on the intensity at MBA and PS characteristic peaks (1078 and 1003 cm^{-1}). The areas with clear MBA SERS signals were then further investigated at higher magnification: in each area, the particles were identified by recovering the SERS signals using a 100× (Leica Fluotar NA = 0.9) objective, with the He−Ne laser with excitation wavelength at 633 nm and varying acquisition times (Figure 3A). All experiments were run at ambient temperature. Matlab (MathWorks, Inc.), version R2022b, was used for data manipulation and figures preparation.

2.6. Sample Preparation and SERS Detection of Real Samples. A sample of water from the Atlantic Ocean was collected by grab-sampling on a glass tank, approximately at the coordinates 35° 54.968′ N and 17° 42.928′ W and used as a representative of an environmental sample. 100 mL of oceanic water, without any preliminary treatment, was filtered on an aluminum oxide filter (0.2 μm, 23 mm diameter, ANODISC Anopore Inorganic Membrane, Whatman, Merck Darmstadt Germany). The filter was then rinsed three times with 20 mL of Milli-Q water to eliminate excess salt and before the addition of 30 mL of AuNS-MBA solution (30 mL of Milli-Q water with the addition of 100 μL of AuNS-MBA 8.33 pM) on top of the filter. About 0.5 mL of HCl 0.1 M was added to adjust the pH to about 5. The whole system was kept under stirring for an hour before filtering the excess solution. The first quick scan (quick map) was conducted with a 10× (N.A. 0.25) objective and 785 nm excitation wavelength on an area of 1 × 1 mm^2 with a step size of 10 μm. Each spectrum was acquired for 5 s at 3 mW laser power. Baseline correction and cosmic ray removal were done with WiRe 4.4 software, and the results were then elaborated using Matlab R2019b and R2022b, based on the intensity at the MBA characteristic peak at 1078 cm^{-1}. The areas with clear MBA SERS signals (signal-to-noise ratio over 2, Figure S18) were then further investigated at higher magnification. Microplastic particles were identified over the selected areas by recovering the SERS signals using a 100× (Leica Fluotar NA = 0.9) objective with the He−Ne laser with an excitation wavelength of 633 nm. A reduced spectral range (200−2000 cm^{-1}) was adopted to optimize measurement times.[56,57] The acquired spectra were then compared with a library of environmentally aged microplastics[58] (Figure 4A). All experiments were run at ambient temperature.

3. RESULTS AND DISCUSSION

3.1. Nanostars Synthesis and Characterization. Aggregates of Au nanospheres,[39,59] as well nanorods[60] and nanostars[61] are all excellent colloidal plasmonic substrates for SERS. Due to their strong SERS enhancement within their limited dimensions, gold nanostars are particularly suitable for labeling small particles like micro- and nanoplastics. The AuNS herein synthesized by the seed-growing approach have a size distribution of about 100 nm (determined by TEM, Figure S1B), and bright SERS enhancements, thanks to the hotspots localized on their spikes.[62] MBA is often used in SERS applications due to its strong SERS signals (Figure S1C).[52] Indeed, the carboxylic acid functionalities (pK_a = 6.3)[63] provide a tunable hydrophobicity to the nanostructures. MBA becomes hydrophilic at neutral and basic pH, due to the presence of the deprotonated form of the molecule, which is

https://doi.org/10.1021/acsomega.4c05693
ACS Omega 2024, 9, 40821−40831

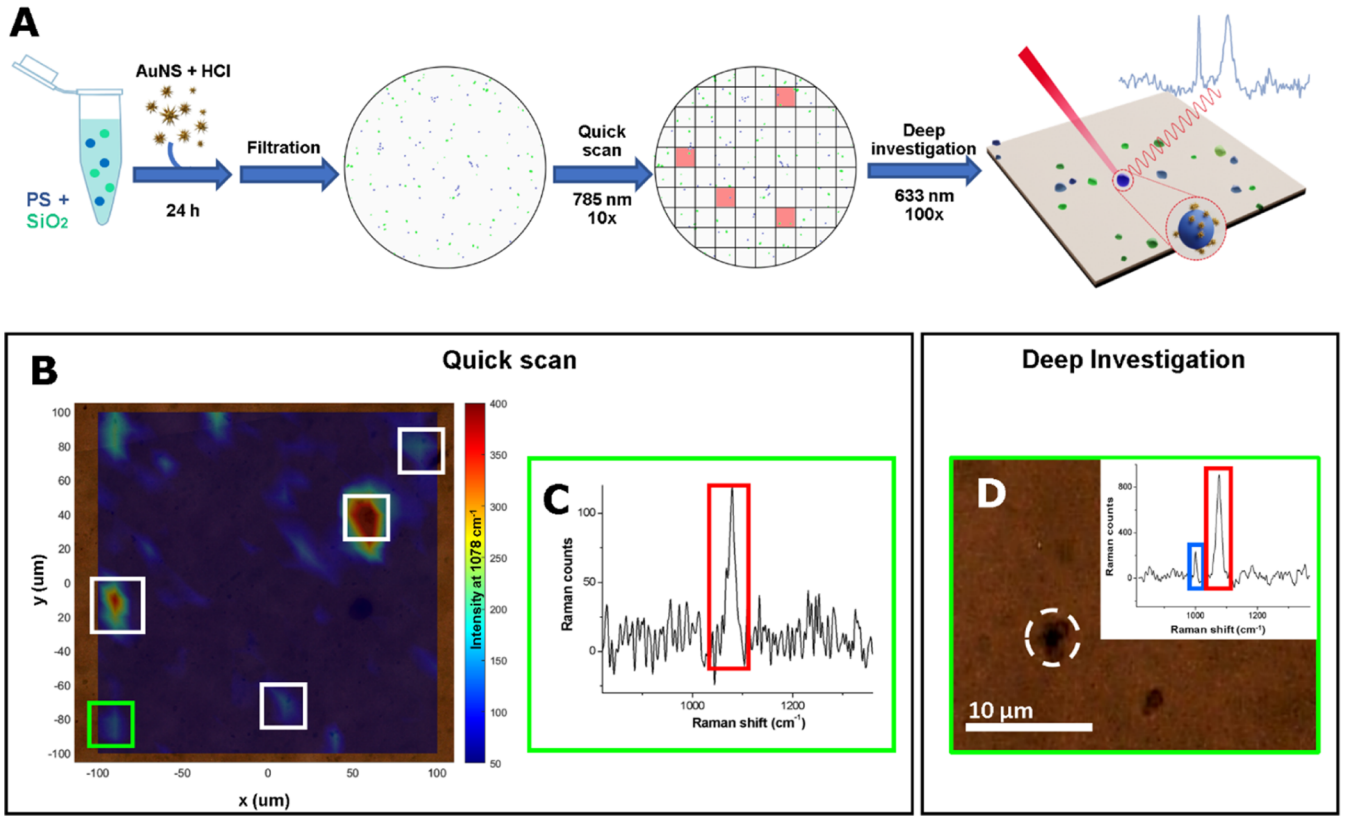

Figure 3. (A) Schematic representation of the method applied on alumina filter for labeling PS nanobeads with AuNS-MBA. (B) Raman imaging (quick map) of PS and SiO_2 nanobeads labeled with AuNS-MBA. A 10× objective and 785 nm excitation wavelength were used. The area is reported as false colored according to intensities at 1078 cm^{-1} (MBA, B). An example of an area that was then selected for further investigation is highlighted by the green box. The spectrum acquired during the quick scan with a clear AuNS-MBA SERS peak is shown in (C). The same area is then further inspected with the 100× objective (D) showing the presence of a PS nanobead tagged with the nanostars, as confirmed by the Raman spectra (633 nm excitation), where the MBA and PS peaks are marked in red and blue, respectively. The other areas selected in (B) can be found in Figure S16.

confirmed by the intensity increasing of the band at about 1420 cm^{-1} with respect to that of the band at about 1720 cm^{-1} (Figure S1C).[52] It constitutes an advantage for the stabilization of gold nanostars dispersion in water because of the Coulomb repulsion.[64] On the other hand, the hydrophobicity of MBA-functionalized AuNS at acidic pH[48] is herein used to selectively interact with the, mostly, hydrophobic micro- and nanoplastics. A general mechanism is assumed due to the presence of hydrophobic and $\pi-\pi$ interactions between the MBA-functionalized AuNS (in their protonated form at slightly acidic pH) and the PS nanospheres, used as a representative for others, as evidenced by the clear localization of MBA signals in the proximity of PS beads only at acidic pH (Figure S4).

3.2. Selective Labeling of PS, LDPE, PET, PTFE, PA6, and PA12 Microplastics with AuNS-MBA. Among the most common artificial nanoplastics, used as models, polystyrene nanobeads of about 800 nm are found to be of great convenience.[28,30,41,65−67] In fact, polystyrene nanobeads can be easily produced with controlled sizes, and the size chosen for this test is still sufficient to provide clear and distinguishable Raman bands and be visible by optical microscopy with high-magnification objectives. Moreover, polystyrene is an environmentally relevant polymer commonly found in environmental samples of surface and upper water column samples due to its buoyancy. For these reasons, they were selected as the main model analyte for the calibration of the present selective SERS labeling approach. The principle underlying the selective interaction of AuNS-MBA with PS is the tunable hydrophobicity of AuNS-MBA due to the protonation equilibrium of MBA,[52] clearly represented by the characteristic spectral changes in Figure S1C. As sketched in Figure 1A, the hydrophobicity of AuNS-MBA is expected to increase at pH 6 and below, so one expects that they preferentially assemble on the PS and not on SiO_2 nanobeads. The spectrum in Figure 1B was registered on a PS bead after the addition of the gold nanostars (AuNS:PS proportion was 12:1) and shows both the PS (Raman) and MBA (SERS) signals. They are found, respectively, at 1003 cm^{-1} for polystyrene and at 1078 cm^{-1} for MBA, well separated and with comparable intensities. Several polystyrene Raman signals are visible, and the spectrum of the polymer is clearly recognizable. Instead, the silica particles, when investigated using point-by-point μ-Raman measurements, do not present any characteristic Raman peaks. On the other hand, the absence of interaction of AuNS-MBA with the SiO_2 surface can be evidenced by the absence of the SERS signals near to the SiO_2 particles.

The SEM image presented in Figure 1C (additional images with EDS analysis in Figure S5) shows the presence of AuNS-MBA distributed around the PS spheres. AuNS-MBA is visible as brighter spots because of the higher electron density of Au compared with that of polystyrene. The same cannot be found on the surface of SiO_2 nanobeads (Figure S5). The mixtures

https://doi.org/10.1021/acsomega.4c05693
ACS Omega 2024, 9, 40821−40831

composed of AuNS-MBA and PS, or SiO_2, particles were finally drop-cast on a glass slide and μ-Raman maps were registered over about a 1.5×10^4 μm^2 area, with a lateral resolution of 1 μm (Figures 2A,B and S6). The number of AuNS-MBA particles was set to 23:1 with respect to that of the PS or SiO_2 nanobeads. MBA signals were found to be almost 1 order of magnitude stronger on PS particles than on SiO_2 particles (Figure 2A,B). A deeper inspection showed that only a few SiO_2 nanobeads report pale MBA signals, most of the time barely distinguishable with respect to background noise (Figures 2B and S6C). It must be recalled that the experimental setup does not account for cleaning the glass slide once drop-cast, so the absence of the SERS signal on the background is also worth noting (Figure S6A,C). Even if a clean background may be expected for PS particles, where selective binding allows AuNS-MBA to accumulate over polymeric nanobeads, it is not the case for SiO_2. μ-Raman inspections in the coffee-ring region for the two samples reveal the fate of the AuNS-MBA nanostructures: the signals are much stronger in the SiO_2 coffee-ring region (Figure S7). Instead, the coffee-ring region on polystyrene does not appear much different from the center of the drop-cast sample. These results show that the AuNS-MBA do not significantly interact with SiO_2 nanobeads; therefore, they are more likely to migrate toward the coffee-ring region during solvent evaporation.

The selectivity of the interaction of AuNS-MBA with PS, as well as the optimal amount of AuNSs, were evaluated by mapping between 100 and 200 single PS and SiO_2 nanobeads after incubation with different amounts of AuNS-MBA. Intensities at the characteristic peaks of MBA (1078 cm^{-1}) and PS (1003 cm^{-1}), together with Pearson's correlation coefficients with MBA and PS reference spectra (R_{MBA} and R_{PS} in the following) were used as figures of merit (Figures 2C and S8). Pearson correlation is a well-established method for checking for the correspondence of an unknown within a library of reference spectra, and it is intended as a qualitative criterion. On the other hand, monitoring the intensities of one or more characteristic peaks is prone to false positives, but does indeed provide a more quantitative view of the amount of AuNS-MBA on each PS or SiO_2 nanobead.[61] Therefore, a clear description of "what" and "how much" is appropriately given using both descriptors. The average R_{MBA} for the spectra measured on PS nanobeads increases with the amount of AuNS-MBA, while the opposite trend is observed for R_{PS} (Figures 3C and S8−S11). Attributions by Pearson correlations may, in fact, be influenced when a spectrum is composed of multiple overlapping traces (i.e., different substances). Since the spectra acquired on PS spheres contain signals from AuNS (so MBA) and from PS, R_{MBA} is smaller when PS dominates the spectrum, and *vice versa*. The spectra acquired on SiO_2 nanoparticles also show a clear monotonic increase in R_{MBA} with the amount of AuNS (Figures 3C, S8, S10, and S11). However, R_{MBA} on SiO_2 particles is systematically lower than those on PS particles, even though SiO_2 cannot lower the correlation values by the already cited overlapping effect. The intensities of the MBA SERS signal (at 1078 cm^{-1}), measured on polystyrene particles, also increase with the amount of AuNS, as expected (Figures 3C,D, S9, and S11). On the contrary, the intensity of the most characterizing PS peak (1003 cm^{-1}) is not affected by the amount of AuNS-MBA, and its value does not vary significantly (Figures 3C,D, S9, S11, and S12). This indicates that the two spectral contributions, from AuNS-MBA and PS, are additive, and therefore, the spectrum of the PS polymer is always recognizable and not affected even at the highest AuNS-MBA dosage. MBA intensities on SiO_2 particles also increase with higher doses, but to a much lower extent. The difference between PS and SiO_2 nanobeads becomes progressively more evident by increasing the AuNS-MBA amount (Figures 3C,D and S8). As stated previously, Pearson correlations and Raman/SERS band intensities are both useful descriptors for assessing labeling selectivity. The PS labeling yield was estimated in Figure S12 as 84.9% for the dosage ratio of particles equal to 23, considering the distribution of both the MBA band intensities and the related R_{MBA} compared to the unlabeled sample (refer to the Supporting Information for details about labeling yield estimation). A limited unspecific AuNS-MBA adhesion on SiO_2 is revealed by the R_{MBA} (Figures S8 and S10). However, the associated MBA spectral intensities are about 1 order of magnitude lower on SiO_2 particles with respect to the PS ones, as one can see in Figure 3C for the 12:1 dosage, resumed for all of the dosages in the boxplots of Figure S9 and scatterplots of Figure S11. All of these suggest that the hydrophobicity of AuNS-MBA, at acidic pH, results in a selective interaction between AuNS-MBA and hydrophobic nanoplastics, with respect to inorganic, i.e., more hydrophilic, ones. A qualitative evaluation of the affinity of these SERS-tags with different microplastics (namely, made of other polymers) was also performed (Figure S13). 2 mg of five other different microplastics (PE, PET, PTFE, PA6, and PA12) were incubated for 24 h with 100 μL of AuNS-MBA, and then deposited on an aluminum surface. SEM images were acquired to verify the presence of the tags on the surface of the microplastics. Then, Raman spectra (with 633 and 785 nm excitation wavelength) were acquired on the surface of the same microplastics, to verify the presence of the signals of the SERS-tags, as well as to investigate how these signals overlap with the Raman of the polymer. Overall, all microplastics clearly showed the presence of the AuNS-MBA SERS-tags on their surfaces in the SEM images. The SERS signals were also always present on their surface and were more intense and visible with a 785 nm excitation wavelength (this was especially evident with LDPE and PET, Figure S13). On the other hand, the 633 nm wavelength was more suitable for detecting the Raman signals for those polymers whose characteristic peaks always allowed chemical speciation.

3.3. Detection of PS Nanobeads Mixed with Silica on Alumina Filter. The time required for microplastic analysis strongly depends on the size of the particles under investigation. The state of the art in nanoplastics detection in practical environmental monitoring is severely limited by two principal issues: the lack of suitable isolation and collection protocols and the extremely time-consuming measures. The following section addresses specifically the latter, taking advantage of the selective interaction between AuNS-MBA and PS nanobeads, again used as model nanoplastic. Along with the microspectroscopic techniques, μ-Raman is the most promising for nanoplastics, thanks to the visible lasers used for the excitation, providing sampling in smaller focal volume under the microscope. Nevertheless, nanoplastics are barely distinguishable by optical microscopes on the filter surface, where they are collected. Because of that, multiple filter portions must be entirely mapped at a suitable resolution for nanoplastics, namely, at least by 1 μm spaced grid. This leads to a huge number of spectra, which typically will be mostly discharged as not reporting any useful signal

https://doi.org/10.1021/acsomega.4c05693
ACS Omega 2024, 9, 40821−40831

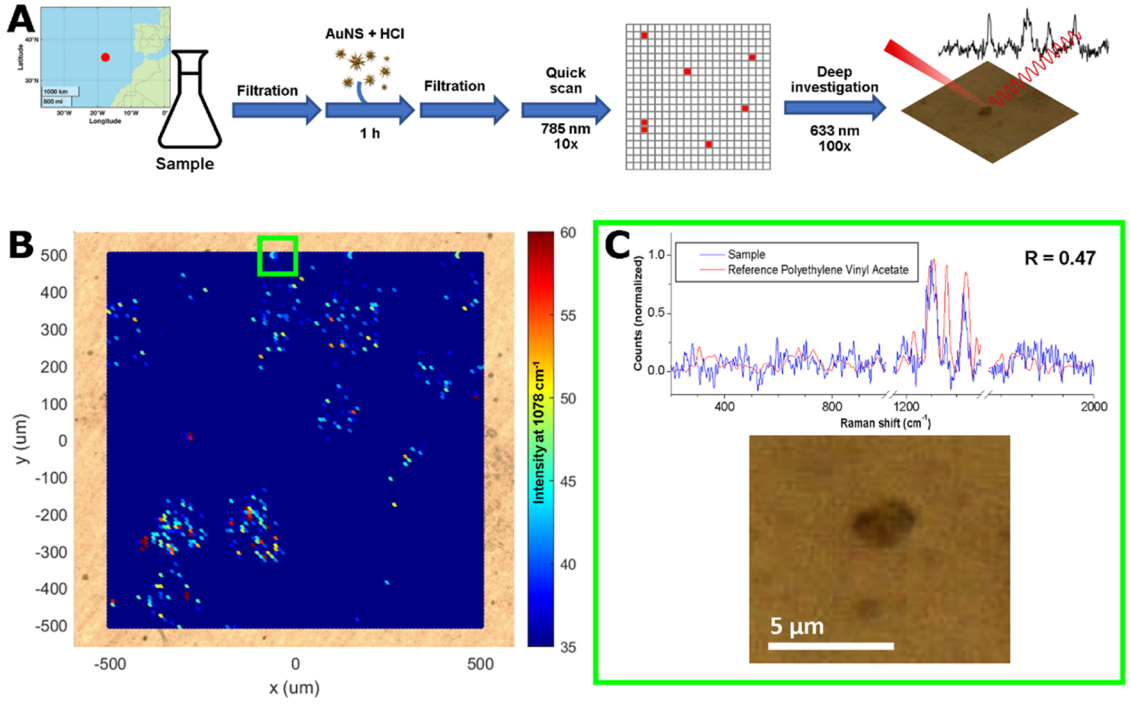

Figure 4. (A) Schematic representation of the method applied to the sample of oceanic water, with the map representing the point of sampling. (B) Map in false color of the intensities of the signals of AuNS-MBA at 1078 cm^{-1} detected during the quick scan. A 10× objective and 785 nm excitation wavelength were used (10 s, 3 mW). An example of an area that was then selected for further investigation is highlighted by the green box. The same area is then further inspected with the 100× objective; (C) the spectrum (633 nm, 0.01 mW, 10 s) of the particle identified is shown overlapped with the reference spectrum.

(i.e., not any nanoplastics). This intrinsically inefficient and time-consuming approach has been herein overpassed due to the selective labeling of the nanoplastics with AuNS-MBA. It makes it possible to scan a large area at 10 times less magnification along the *x* and *y* axes. This results in 100 times less spectra to acquire to indirectly localize the nanoplastics by the signals associated with the SERS-tags. The PS and SiO_2 nanobeads were mixed at equivalent amounts and incubated with AuNS-MBA (23:1 ratio) before being collected by filtration under vacuum on alumina filters (0.4 μm filter pores). Due to the bright SERS signals provided by AuNS-MBA, a fast map at low resolution (herein referred to as *quick map*) allows us to indirectly recover the PS nanobeads location through the filter surface. This setup is not sufficient to collect the Raman signals of PS, but due to the selective interaction of AuNS-MBA with PS, the last are eventually located for a subsequent inspection at a higher magnification. The overall method is sketched in Figure 3A.

The quick map is obtained using a 10× objective, which allows coverage of a larger area in a short time. A 785 nm excitation line was also chosen, since it yields higher SERS intensities by AuNS-MBA due to the better resonance with the nanostars plasmon band compared to the 633 nm excitation (Figure S14). A filter area as large as about 200 × 200 μm^2 was mapped at 10 μm resolution in about 1 h (quick map) and reported in false colors representing the intensities of the characteristic peaks of MBA and PS (Figures 3B and S15). Not any PS Raman band can be spotted on the map, whereas many areas show high intensities at 1078 cm^{-1}, corresponding to the AuNS-MBA SERS signals (Figure 3C). The mapping resolution used for the quick map is not sufficient to distinguish between aggregates and single nanobeads (PS or SiO_2), so it results in high variability along the measured MBA signal intensities (Figure 3B). Nevertheless, one can recall that the quick map has a qualitative and screening purpose so that all of the points with recognizable MBA bands (no matter the intensity) are selected to be further inspected at higher magnification. The areas selected during the quick map are then measured again using a 100× magnification objective and 633 nm laser excitation (Figures 3D and S16). This time, both the AuNS-MBA SERS peak and the PS Raman peak (at 1003 cm^{-1}) are clearly recognizable. This further underlines that the AuNS-MBA labeling does not prevent the recognition of the polymer spectrum (PS in this case). Figure S16 shows other areas along the *quick map* selected due to the MBA SERS signal. Both PS and MBA bands can be recognized in most of them, except for the particle in Figure S16E. The lack of PS signals may lead to the conclusion that the nanobead in Figure S16E is made of SiO_2 so that a potential false positive is avoided due to the double check on both MBA SERS and PS Raman bands. It is also worth noting that the present approach ultimately makes it possible to detect single polystyrene nanobeads (down to 800 nm) on alumina filters with a 10× magnification in about 1 h. As a comparison, to scan the same area (200 × 200 μm^2) directly at the highest magnification,[28,56−58] the number of spectra to acquire, and consequently the measurement time, would be about 100 times higher (a grid with an edge of 1 μm would be needed). Another test was conducted as a scale-up experiment before the application to real samples (Figure S17). 100 mL of Milli-Q water was spiked with PS nanobeads. This time, the sample was filtered on the alumina filter before the addition of the SERS-tags to preconcentrate the particles, according to the common practice in environmental microplastic monitoring. The AuNS-MBA were then added on top of the filter and kept in contact for 1 h under mild stirring. The quick scan and the

https://doi.org/10.1021/acsomega.4c05693
ACS Omega 2024, 9, 40821−40831

following deeper investigation were then conducted as previously, but this time on a bigger surface (1 × 1 mm^2). Once again, it was possible to identify single nanoplastics (Figure S17).

3.4. Application to Environmental Samples. The application to real samples comes with new challenges related to the potential presence of many different microplastics, composed of different polymers, as well as the presence of different interferents and a bigger volume of the sample. To address the latter issue, and according to the last section and the scheme in Figure 4A, the microplastics were preconcentrated by filtration on alumina filters, and the SERS-tags were therefore added. The mixture was kept under mild stirring to ensure the lifting of the microplastics from the surface of the filter and proper mixing and interaction with the SERS-tags. A second filtration ensured drainage of the SERS-tags in excess, and the analysis was then conducted with the conditions that were optimized with the fabricated samples: a quick scan using a 785 nm excitation wavelength and 10× objective, covering a whole area of 1 × 1 mm^2 with a 10 μm grid, followed by a deeper analysis at 633 nm excitation and 100× objective of the areas showing a significant MBA signal. These areas were selected based on the intensity at 1078 cm^{-1}, related to the SERS peak of MBA (Figure 4B). An intensity of 35 Raman counts and a signal-to-noise threshold of minimum 2 were chosen, which were the limits allowing the MBA signals to be clearly discerned from the background noise (some examples are reported in Figure S18). The selected areas were then further analyzed: the particles were manually selected, and a Raman spectrum was acquired on each of them. With respect to the previous cases, in which the nanoplastics were artificially spiked, the obtained spectra were now compared to a library of environmentally aged microplastics.[68] On each spectrum, portions between 1040 and 1140 cm^{-1} and between 1510 and 1660 cm^{-1}, corresponding to the SERS peaks of MBA, were cut to avoid false attributions. Pearson correlation (R) was used again as a parameter to evaluate the best match. Many areas were selected during the quick scan; however, only a few particles showed significant signals that could match the spectra from the library (Figures 4C and S19). An example of a microplastic identified with this method is reported in Figure 4C, and the microplastic identified was a polyethylene-polyvinyl acetate copolymer with a size of about 2 μm. PE−PVA is a copolymer, so the different relative intensities of the Raman peaks can be attributed to different percentages of each polymer component compared to the reference library. It is indeed well known how the natural aging of microplastic, together with the presence of copolymers, additives, absorbents, and so on, may cause a lower attribution percentage match with respect to the library references.[58] Other microplastics and nonplastic particles, identified within the same experiment, are reported in Figure S19. The spectrum in Figure S19A shows a great match (R > 0.9) with the reference spectra of polyethylene. However, the signals can be attributed to Rutile, the most common titanium dioxide mineral. Rutile is also used as a white pigment and filler for plastics, and its signals could prevail over the one from the plastic itself; however, without the characteristic peaks from the polymer, it is not possible to discern if the signal is due to an inorganic particle itself or a microplastic containing rutile as an additive.

It should be noted that a proper SERS-tags/microplastic is not possible to set for an unknown sample. Figures 2D, S8, and S9 show dose/response curves for different SERS-tags/nanoplastics amounts, in terms of molar ratios. These data clearly demonstrate that a 20-fold excess of SERS-tags does not prevent the recovery of nanoplastic polymer Raman signals, indeed of great importance for nanoplastic identification and simultaneous detection of false positives (Figure S16E). When applied to real samples, where the concentration of nanoplastics is unknown, a much higher SERS-tags excess may be expected. The fate of the SERS-tags in excess is therefore supposed to be (i) a higher loading of SERS-tags at each microplastic according to Figure 2D, (ii) the SERS-tags in excess can be filtered out according to the procedure scheme in Figure 4A, and (iii) the SERS-tags in excess can be retained at the filter as false positive in the quick map, eventually discharged thanks to the deep inspection at higher magnification. In any case, it will not result in a failure of the overall method.

These results report a small number of microplastics identified in the aliquot of the offshore Atlantic Ocean surface water. The limited sampled volume and relatively small geographical area considered are not sufficient for a robust quantitative microplastic estimation, indeed out of the scope of this study. Nevertheless, these proof-of-concept, qualitative results provide a significant first step toward the application of this labeling technique to the environmental analysis of micro- and nanoplastics. Further efforts toward extensive implementation are needed to advance this method to environmental monitoring campaigns. For example, factors such as the impact of sample cleaning and pretreatment, as well as the potential bias toward some polymers, should impact the limit of detection, for instance, and will be evaluated in dedicated future studies.

4. CONCLUSIONS

Within the context of microplastic environmental pollution, the nanoplastic fraction is still, nowadays, the most challenging target to address because of methodological and technological issues. MBA-functionalized AuNS have a tunable hydrophobicity that is herein used to selectively assemble them on hydrophobic microplastics down to nanobeads of 800 nm. This interaction was found effectively useful for labeling microplastics (i.e. PS, LDPE, PET, PTFE, PA6, and PA12) with respect to inorganic (i.e., SiO_2) particles of the same dimension, underlying a clear selectivity of the target analyte. The application of these tags to microplastic analysis foresees the adoption of alumina filters, according to a well-established practice in environmental microplastic monitoring. A prescreening, fast μ-Raman map at lower magnification allows us to locate the micro- and nanoplastics due to the intense SERS fingerprint provided by the AuNS-MBA labels. The Raman signals of the polymers are subsequently recovered by higher-magnification inspection, providing a double check against false-positive attributions, and allowing the chemical speciation of the microplastics. The method was further validated on environmental samples of oceanic offshore surface water, with the worth-noting result of the detection of small microplastic particles. The comprehensive set of calibration and validation experiments herein presented pave the way for a potential future implementation of the same approach on a microplastic monitoring campaign.

https://doi.org/10.1021/acsomega.4c05693
ACS Omega 2024, 9, 40821−40831

■ ASSOCIATED CONTENT

Supporting Information

The Supporting Information is available free of charge at https://pubs.acs.org/doi/10.1021/acsomega.4c05693.

UV−vis spectra of colloids, SEM and TEM images, labeling activity at acidic/basic conditions, additional μ-Raman imaging, additional Pearson's correlation coefficient and bands intensities plots, protocol and additional measures for particles quantification, dosages, and labeling activity (PDF)

■ AUTHOR INFORMATION

Corresponding Author

Lucio Litti − *Department of Chemical Sciences, University of Padova, 35131 Padova, Italy;* orcid.org/0000-0001-6247-5456; Email: lucio.litti@unipd.it

Authors

Anna Mercedi − *Department of Chemical Sciences, University of Padova, 35131 Padova, Italy*

Giulia Gentili − *Department of Chemical Sciences, University of Padova, 35131 Padova, Italy*

Valentina Poli − *DICEA, Department of Civil, Environmental and Architectural Engineering, University of Padua, 35131 Padova, Italy;* orcid.org/0000-0001-5827-7107

Carolin Philipp − *Fram Centre, Norwegian Polar Institute, Tromsø 9296, Norway;* orcid.org/0000-0003-0000-7037

Beatrice Rosso − *Institute of Polar Sciences, CNR-ISP, 30172 Venezia-Mestre, Italy; Department of Environmental Sciences, Informatics, and Statistics, DAIS, Campus Scientifico, Ca'Foscari University of Venice, 30172 Venezia-Mestre, Italy*

Maria Cristina Lavagnolo − *DICEA, Department of Civil, Environmental and Architectural Engineering, University of Padua, 35131 Padova, Italy*

Ingeborg Hallanger − *Fram Centre, Norwegian Polar Institute, Tromsø 9296, Norway*

Fabiana Corami − *Institute of Polar Sciences, CNR-ISP, 30172 Venezia-Mestre, Italy; Department of Environmental Sciences, Informatics, and Statistics, DAIS, Campus Scientifico, Ca'Foscari University of Venice, 30172 Venezia-Mestre, Italy*

Moreno Meneghetti − *Department of Chemical Sciences, University of Padova, 35131 Padova, Italy;* orcid.org/0000-0003-3355-4811

Complete contact information is available at: https://pubs.acs.org/10.1021/acsomega.4c05693

Author Contributions

A.M. was in charge of nanostars synthesis, A.M. and G.G. for data acquisition and curation. G.G. synthesized the silica particles. B.R. and F.C. provided methodology for filtering in alumina filters. L.L. accounted for conceptualization and supervision. C.P. and I.H. provided labeling with other microplastics instead of PS. V.P. and M.C.L. provided real samples from Atlantic Ocean. All of the authors contributed to the results discussion and manuscript writing.

Notes

The authors declare no competing financial interest.

■ ACKNOWLEDGMENTS

L.L. acknowledges the Italian Ministry of Education, Universities and Research through the project entitled "Nanochemistry for Energy and Health, NExuS" (the national funding network termed "Dipartimenti di Eccellenza" awarded to the Department of Chemical Sciences at the University of Padua).

■ REFERENCES

(1) Choong, W. S.; Hadibarata, T.; Yuniarto, A.; Tang, K. H. D.; Abdullah, F.; Syafrudin, M.; Al Farraj, D. A.; Al-Mohaimeed, A. M. Characterization of Microplastics in the Water and Sediment of Baram River Estuary, Borneo Island. *Mar. Pollut. Bull.* **2021**, *172*, No. 112880.

(2) Caldwell, J.; Taladriz-Blanco, P.; Lehner, R.; Lubskyy, A.; Ortuso, R. D.; Rothen-Rutishauser, B.; Petri-Fink, A. The Micro-, Submicron-, and Nanoplastic Hunt: A Review of Detection Methods for Plastic Particles. *Chemosphere* **2022**, *293*, No. 133514.

(3) Jin, N.; Song, Y.; Ma, R.; Li, J.; Li, G.; Zhang, D. Characterization and Identification of Microplastics Using Raman Spectroscopy Coupled with Multivariate Analysis. *Anal. Chim. Acta* **2022**, *1197*, No. 339519.

(4) Malankowska, M.; Echaide-Gorriz, C.; Coronas, J. Microplastics in Marine Environment: A Review on Sources, Classification, and Potential Remediation by Membrane Technology. *Environ. Sci.: Water Res. Technol.* **2021**, *7* (2), 243−258.

(5) World Health Organization. *Dietary and Inhalation Exposure to Nano- and Microplastic Particles and Potential Implications for Human Health*, 2022.

(6) Wright, S. L.; Thompson, R. C.; Galloway, T. S. The Physical Impacts of Microplastics on Marine Organisms: A Review. *Environ. Pollut.* **2013**, *178*, 483−492.

(7) Van Cauwenberghe, L.; Claessens, M.; Vandegehuchte, M. B.; Janssen, C. R. Microplastics Are Taken up by Mussels (Mytilus Edulis) and Lugworms (Arenicola Marina) Living in Natural Habitats. *Environ. Pollut.* **2015**, *199*, 10−17.

(8) Hurley, R. R.; Woodward, J. C.; Rothwell, J. J. Ingestion of Microplastics by Freshwater Tubifex Worms. *Environ. Sci. Technol.* **2017**, *51* (21), 12844−12851.

(9) Zhang, Y.; Lu, J.; Wu, J.; Wang, J.; Luo, Y. Potential Risks of Microplastics Combined with Superbugs: Enrichment of Antibiotic Resistant Bacteria on the Surface of Microplastics in Mariculture System. *Ecotoxicol. Environ. Saf.* **2020**, *187*, No. 109852.

(10) Prata, J. C.; da Costa, J. P.; Lopes, I.; Duarte, A. C.; Rocha-Santos, T. Environmental Exposure to Microplastics: An Overview on Possible Human Health Effects. *Sci. Total Environ.* **2020**, *702*, No. 134455.

(11) Kooi, M.; Primpke, S.; Mintenig, S. M.; Lorenz, C.; Gerdts, G.; Koelmans, A. A. Characterizing the Multidimensionality of Microplastics across Environmental Compartments. *Water Res.* **2021**, *202*, No. 117429.

(12) Silva, A. B.; Bastos, A. S.; Justino, C. I. L.; da Costa, J. P.; Duarte, A. C.; Rocha-Santos, T. A. P. Microplastics in the Environment: Challenges in Analytical Chemistry - A Review. *Anal. Chim. Acta* **2018**, *1017*, 1−19.

(13) Shruti, V. C.; Pérez-Guevara, F.; Elizalde-Martínez, I.; Kutralam-Muniasamy, G. Current Trends and Analytical Methods for Evaluation of Microplastics in Stormwater. *Trends Environ. Anal. Chem.* **2021**, *30*, No. e00123.

(14) Yao, Y.; Glamoclija, M.; Murphy, A.; Gao, Y. Characterization of Microplastics in Indoor and Ambient Air in Northern New Jersey. *Environ. Res.* **2022**, *207*, No. 112142.

(15) Rosso, B.; Gregoris, E.; Litti, L.; Zorzi, F.; Fiorini, M.; Bravo, B.; Barbante, C.; Gambaro, A.; Corami, F. Identification and Quantification of Tire Wear Particles by Employing Different Cross-Validation Techniques: FTIR-ATR Micro-FTIR, Pyr-GC/MS, and SEM. *Environ. Pollut.* **2023**, *326*, No. 121511.

(16) Poli, V.; Lavagnolo, M. C.; Barausse, A.; Benetello, E.; Palmeri, L. WAste Characterization In The Urban Canal Network Of Padova (Italy) To Mitigate Downstream Marine Plastic Pollution. *Detritus* **2023**, *22*, 99.

(17) Alfaro-Núñez, A.; Astorga, D.; Cáceres-Farías, L.; Bastidas, L.; Soto Villegas, C.; Macay, K. C.; Christensen, J. H. Microplastic Pollution in Seawater and Marine Organisms across the Tropical Eastern Pacific and Galápagos. *Sci. Rep.* **2021**, *11* (1), No. 6424.
(18) Corami, F.; Rosso, B.; Sfriso, A. A.; Gambaro, A.; Mistri, M.; Munari, C.; Barbante, C. Additives, Plasticizers, Small Microplastics (<100 Mm), and Other Microlitter Components in the Gastrointestinal Tract of Commercial Teleost Fish: Method of Extraction, Purification, Quantification, and Characterization Using Micro-FTIR. *Mar. Pollut. Bull.* **2022**, *177*, No. 113477.
(19) Corami, F.; Rosso, B.; Roman, M.; Picone, M.; Gambaro, A.; Barbante, C. Evidence of Small Microplastics (<100 Mm) Ingestion by Pacific Oysters (Crassostrea Gigas): A Novel Method of Extraction, Purification, and Analysis Using Micro-FTIR. *Mar. Pollut. Bull.* **2020**, *160*, No. 111606.
(20) Iannilli, V.; Pasquali, V.; Setini, A.; Corami, F. First Evidence of Microplastics Ingestion in Benthic Amphipods from Svalbard. *Environ. Res.* **2019**, *179* (Pt A), No. 108811.
(21) Jiang, Y.; Yang, F.; Hassan Kazmi, S. S. U.; Zhao, Y.; Chen, M.; Wang, J. A Review of Microplastic Pollution in Seawater, Sediments and Organisms of the Chinese Coastal and Marginal Seas. *Chemosphere* **2022**, *286* (Pt 1), No. 131677.
(22) Wang, W.; Ge, J.; Yu, X. Bioavailability and Toxicity of Microplastics to Fish Species: A Review. *Ecotoxicol. Environ. Saf.* **2020**, *189*, No. 109913.
(23) Bai, C.-L.; Liu, L.-Y.; Hu, Y.-B.; Zeng, E. Y.; Guo, Y. Microplastics: A Review of Analytical Methods, Occurrence and Characteristics in Food, and Potential Toxicities to Biota. *Sci. Total Environ.* **2022**, *806*, No. 150263.
(24) Ragusa, A.; Svelato, A.; Santacroce, C.; Catalano, P.; Notarstefano, V.; Carnevali, O.; Papa, F.; Rongioletti, M. C. A.; Baiocco, F.; Draghi, S.; D'Amore, E.; Rinaldo, D.; Matta, M.; Giorgini, E. Plasticenta: First Evidence of Microplastics in Human Placenta. *Environ. Int.* **2021**, *146*, No. 106274.
(25) Çobanoğlu, H.; Belivermiş, M.; Sıkdokur, E.; Kılıç, Ö.; Çayır, A. Genotoxic and Cytotoxic Effects of Polyethylene Microplastics on Human Peripheral Blood Lymphocytes. *Chemosphere* **2021**, *272*, No. 129805.
(26) Xu, J.-L.; Thomas, K. V.; Luo, Z.; Gowen, A. A. FTIR and Raman Imaging for Microplastics Analysis: State of the Art, Challenges and Prospects. *TrAC, Trends Anal. Chem.* **2019**, *119*, No. 115629.
(27) Anger, P. M.; von der Esch, E.; Baumann, T.; Elsner, M.; Niessner, R.; Ivleva, N. P. Raman Microspectroscopy as a Tool for Microplastic Particle Analysis. *TrAC, Trends Anal. Chem.* **2018**, *109*, 214−226.
(28) Sobhani, Z.; Zhang, X.; Gibson, C.; Naidu, R.; Megharaj, M.; Fang, C. Identification and Visualisation of Microplastics/Nanoplastics by Raman Imaging (i): Down to 100 Nm. *Water Res.* **2020**, *174*, No. 115658.
(29) Araujo, C. F.; Nolasco, M. M.; Ribeiro, A. M. P.; Ribeiro-Claro, P. J. A. Identification of Microplastics Using Raman Spectroscopy: Latest Developments and Future Prospects. *Water Res.* **2018**, *142*, 426−440.
(30) Qian, N.; Gao, X.; Lang, X.; Deng, H.; Bratu, T. M.; Chen, Q.; Stapleton, P.; Yan, B.; Min, W. Rapid Single-Particle Chemical Imaging of Nanoplastics by SRS Microscopy. *Proc. Natl. Acad. Sci. U.S.A.* **2024**, *121* (3), No. e2300582121.
(31) Levermore, J. M.; Smith, T. E. L.; Kelly, F. J.; Wright, S. L. Detection of Microplastics in Ambient Particulate Matter Using Raman Spectral Imaging and Chemometric Analysis. *Anal. Chem.* **2020**, *92* (13), 8732−8740.
(32) Pittroff, M.; Müller, Y. K.; Witzig, C. S.; Scheurer, M.; Storck, F. R.; Zumbülte, N. Microplastic Analysis in Drinking Water Based on Fractionated Filtration Sampling and Raman Microspectroscopy. *Environ. Sci. Pollut Res.* **2021**, *28* (42), 59439−59451.
(33) Corami, F.; Rosso, B.; Morabito, E.; Rensi, V.; Gambaro, A.; Barbante, C. Small Microplastics (<100 Mm), Plasticizers and Additives in Seawater and Sediments: Oleo-Extraction, Purification, Quantification, and Polymer Characterization Using Micro-FTIR. *Sci. Total Environ.* **2021**, *797*, No. 148937.
(34) Erni-Cassola, G.; Gibson, M. I.; Thompson, R. C.; Christie-Oleza, J. A. Lost, but Found with Nile Red: A Novel Method for Detecting and Quantifying Small Microplastics (1 Mm to 20 Mm) in Environmental Samples. *Environ. Sci. Technol.* **2017**, *51* (23), 13641−13648.
(35) Maes, T.; Jessop, R.; Wellner, N.; Haupt, K.; Mayes, A. G. A Rapid-Screening Approach to Detect and Quantify Microplastics Based on Fluorescent Tagging with Nile Red. *Sci. Rep.* **2017**, *7* (1), No. 44501.
(36) Primpke, S.; Christiansen, S. H.; Cowger, W.; De Frond, H.; Deshpande, A.; Fischer, M.; Holland, E. B.; Meyns, M.; O'Donnell, B. A.; Ossmann, B. E.; Pittroff, M.; Sarau, G.; Scholz-Böttcher, B. M.; Wiggin, K. J. Critical Assessment of Analytical Methods for the Harmonized and Cost-Efficient Analysis of Microplastics. *Appl. Spectrosc.* **2020**, *74* (9), 1012−1047.
(37) Litti, L.; Meneghetti, M. Predictions on the SERS Enhancement Factor of Gold Nanosphere Aggregate Samples. *Phys. Chem. Chem. Phys.* **2019**, *21* (28), 15515−15522.
(38) Litti, L.; Trivini, S.; Ferraro, D.; Reguera, J. 3D Printed Microfluidic Device for Magnetic Trapping and SERS Quantitative Evaluation of Environmental and Biomedical Analytes. *ACS Appl. Mater. Interfaces* **2021**, *13* (29), 34752−34761.
(39) Litti, L.; Colusso, A.; Pinto, M.; Ruli, E.; Scarsi, A.; Ventura, L.; Toffoli, G.; Colombatti, M.; Fracasso, G.; Meneghetti, M. SERRS Multiplexing with Multivalent Nanostructures for the Identification and Enumeration of Epithelial and Mesenchymal Cells. *Sci. Rep.* **2020**, *10* (1), No. 15805.
(40) Xu, G.; Cheng, H.; Jones, R.; Feng, Y.; Gong, K.; Li, K.; Fang, X.; Tahir, M. A.; Valev, V. K.; Zhang, L. Surface-Enhanced Raman Spectroscopy Facilitates the Detection of Microplastics < 1 Mm in the Environment. *Environ. Sci. Technol.* **2020**, *54* (24), 15594−15603.
(41) Chang, L.; Jiang, S.; Luo, J.; Zhang, J.; Liu, X.; Lee, C.-Y.; Zhang, W. Nanowell-Enhanced Raman Spectroscopy Enables the Visualization and Quantification of Nanoplastics in the Environment. *Environ. Sci.: Nano* **2022**, *9*, 542.
(42) Caldwell, J.; Taladriz-Blanco, P.; Rothen-Rutishauser, B.; Petri-Fink, A. Detection of Sub-Micro- and Nanoplastic Particles on Gold Nanoparticle-Based Substrates through Surface-Enhanced Raman Scattering (SERS) Spectroscopy. *Nanomaterials* **2021**, *11* (5), 1149.
(43) Li, D.; Tian, X.; Yang, W.; Wang, X.; Liu, Y.; Shan, J. Hydrophobicity-Driven Self-Assembly of Nanoplastics and Silver Nanoparticles for the Detection of Polystyrene Microspheres Using Surface Enhanced Raman Spectroscopy. *Chemosphere* **2023**, *339*, No. 139775.
(44) Ruan, X.; Xie, L.; Liu, J.; Ge, Q.; Liu, Y.; Li, K.; You, W.; Huang, T.; Zhang, L. Rapid Detection of Nanoplastics down to 20 Nm in Water by Surface-Enhanced Raman Spectroscopy. *J. Hazard. Mater.* **2024**, *462*, No. 132702.
(45) Xie, L.; Gong, K.; Liu, Y.; Zhang, L. Strategies and Challenges of Identifying Nanoplastics in Environment by Surface-Enhanced Raman Spectroscopy. *Environ. Sci. Technol.* **2023**, *57* (1), 25−43.
(46) Dey, T. Microplastic Pollutant Detection by Surface Enhanced Raman Spectroscopy (SERS): A Mini-Review. *Nanotechnol. Environ. Eng.* **2023**, *8* (1), 41−48.
(47) Vélez-Escamilla, L. Y.; Contreras-Torres, F. F. Latest Advances and Developments to Detection of Micro- and Nanoplastics Using Surface-Enhanced Raman Spectroscopy. *Part. Part. Syst. Charact.* **2022**, *39* (3), No. 2100217.
(48) Niu, X.; Yu, L.; Wang, X.; Zhang, Z.; Li, X.; Feng, X.; Wang, W.; Yuan, Z. Acid-Responsive Aggregated SERS Nanoparticles for Improved Tumor Diagnosis. *Mater. Chem. Front.* **2022**, *6* (5), 644−651.
(49) Soursou, V.; Campo, J.; Picó, Y. A Critical Review of the Novel Analytical Methods for the Determination of Microplastics in Sand and Sediment Samples. *TrAC, Trends Anal. Chem.* **2023**, *166*, No. 117190.

https://doi.org/10.1021/acsomega.4c05693
ACS Omega 2024, 9, 40821−40831

(50) Prata, J. C.; Paço, A.; Reis, V.; da Costa, J. P.; Fernandes, A. J. S.; da Costa, F. M.; Duarte, A. C.; Rocha-Santos, T. Identification of Microplastics in White Wines Capped with Polyethylene Stoppers Using Micro-Raman Spectroscopy. *Food Chem.* **2020**, *331*, No. 127323.
(51) Zhang, Z.; Geng, Y.; Zhou, W.; Shao, X.; Lin, H.; Zhou, Y. Development of a Multi-Spectroscopy Method Coupling μ-FTIR and μ-Raman Analysis for One-Stop Detection of Microplastics in Environmental and Biological Samples. *Sci. Total Environ.* **2024**, *917*, No. 170396.
(52) Litti, L.; Reguera, J.; de Abajo, F. J. G.; Meneghetti, M.; Liz-Marzán, L. M. Manipulating Chemistry through Nanoparticle Morphology. *Nanoscale Horiz.* **2020**, *5* (1), 102−108.
(53) Atta, S.; Beetz, M.; Fabris, L. Understanding the Role of AgNO 3 Concentration and Seed Morphology in the Achievement of Tunable Shape Control in Gold Nanostars. *Nanoscale* **2019**, *11* (6), 2946−2958.
(54) Yuan, H.; Khoury, C. G.; Hwang, H.; Wilson, C. M.; Grant, G. A.; Vo-Dinh, T. Gold Nanostars: Surfactant-Free Synthesis, 3D Modelling, and Two-Photon Photoluminescence Imaging. *Nanotechnology* **2012**, *23* (7), No. 075102.
(55) Ghimire, P. P.; Jaroniec, M. Renaissance of Stöber Method for Synthesis of Colloidal Particles: New Developments and Opportunities. *J. Colloid Interface Sci.* **2021**, *584*, 838−865.
(56) Schmälzlin, E.; Moralejo, B.; Rutowska, M.; Monreal-Ibero, A.; Sandin, C.; Tarcea, N.; Popp, J.; Roth, M. M. Raman Imaging with a Fiber-Coupled Multichannel Spectrograph. *Sensors* **2014**, *14* (11), 21968−21980.
(57) Frère, L.; Paul-Pont, I.; Moreau, J.; Soudant, P.; Lambert, C.; Huvet, A.; Rinnert, E. A Semi-Automated Raman Micro-Spectroscopy Method for Morphological and Chemical Characterizations of Microplastic Litter. *Mar. Pollut. Bull.* **2016**, *113* (1), 461−468.
(58) Munno, K.; De Frond, H.; O'Donnell, B.; Rochman, C. M. Increasing the Accessibility for Characterizing Microplastics: Introducing New Application-Based and Spectral Libraries of Plastic Particles (SLoPP and SLoPP-E). *Anal. Chem.* **2020**, *92* (3), 2443−2451.
(59) Ricci, S.; Buonomo, M.; Casalini, S.; Bonacchi, S.; Meneghetti, M.; Litti, L. High Performance Multi-Purpose Nanostructured Thin Films by Inkjet Printing: Au Micro-Electrodes and SERS Substrates. *Nanoscale Adv.* **2023**, *5*, 1970.
(60) Berganza, L. B.; Litti, L.; Meneghetti, M.; Lanceros-Méndez, S.; Reguera, J. Enhancement of Magnetic Surface-Enhanced Raman Scattering Detection by Tailoring Fe3O4@Au Nanorod Shell Thickness and Its Application in the On-Site Detection of Antibiotics in Water. *ACS Omega* **2022**, *7* (49), 45493−45503.
(61) Lenzi, E.; Litti, L.; Jimenez de Aberasturi, D.; Henriksen-Lacey, M.; Liz-Marzán, L. M. SERSTEM: An App for the Statistical Analysis of Correlative SERS and TEM Imaging and Evaluation of SERS Tags Performance. *J. Raman Spectrosc.* **2021**, *52* (2), 355−365.
(62) Hao, F.; Nehl, C. L.; Hafner, J. H.; Nordlander, P. Plasmon Resonances of a Gold Nanostar. *Nano Lett.* **2007**, *7* (3), 729−732.
(63) Yu, X.; Zhong, Y.; Sun, Y.; Chen, Y. Controllable Preparation of Plasmonic Gold Nanostars for Enhanced Photothermal and SERS Effects. *Chem. Res. Chin. Univ.* **2020**, *36* (6), 1284−1291.
(64) Fan, C.; Bian, T.; Shang, L.; Shi, R.; Wu, L.-Z.; Tung, C.-H.; Zhang, T. pH-Responsive Reversible Self-Assembly of Gold Nanoparticles into Nanovesicles. *Nanoscale* **2016**, *8* (7), 3923−3925.
(65) Zhou, X.-X.; Liu, R.; Hao, L.-T.; Liu, J.-F. Identification of Polystyrene Nanoplastics Using Surface Enhanced Raman Spectroscopy. *Talanta* **2021**, *221*, No. 121552.
(66) Hu, R.; Zhang, K.; Wang, W.; Wei, L.; Lai, Y. Quantitative and Sensitive Analysis of Polystyrene Nanoplastics down to 50 Nm by Surface-Enhanced Raman Spectroscopy in Water. *J. Hazard. Mater.* **2022**, *429*, No. 128388.
(67) Yang, Q.; Zhang, S.; Su, J.; Li, S.; Lv, X.; Chen, J.; Lai, Y.; Zhan, J. Identification of Trace Polystyrene Nanoplastics Down to 50 Nm by the Hyphenated Method of Filtration and Surface-Enhanced Raman Spectroscopy Based on Silver Nanowire Membranes. *Environ. Sci. Technol.* **2022**, *56* (15), 10818−10828.
(68) SLoPP and SLoPP-E Raman Spectral Libraries for Microplastics Research. https://plasticactioncentre.ca/directory/slopp-and-slopp-e-raman-spectral-libraries-for-microplastics-research/ (accessed April 26, 2022).

https://doi.org/10.1021/acsomega.4c05693
ACS Omega 2024, 9, 40821−40831